Chapter 2
The EEM in Nipi Structures of Nonparabolic Semiconductors

2.1 Introduction

The concept of doping superlattices (SLs) was introduced by Esaki and Tsu [1] and extensive work in this subject was initiated by Dohler [2–15]. In the compositional SL the periodic potential is due to a change in the band gap of two materials. In doping SLs, the periodicity is space-charge induced and in addition a homogeneous material is used. With the advent of modern experimental techniques of fabricating nanomaterials, it is possible to grow semiconductor SLs composed of alternative layers of two different degenerate layers with controlled thickness. These structures have found wide applications in many new devices such as photodiodes, photoresistors [16], transistors [17], light emitters [18], tunneling devices [19], etc [20–33]. The investigations of the physical properties of narrow gap SLs have increased extensively, since they are important for optoelectronic devices and also since the quality of heterostructures involving narrow gap materials has been greatly improved. It may be noted that the nipi structures, also called the doping superlattices as mentioned above, are crystals with a periodic sequence of ultrathin film layers [19, 20] of the same semiconductor with the intrinsic layer in between together with the opposite sign of doping. All the donors will be positively charged and all the acceptors negatively. This periodic space charge causes a periodic space charge potential which quantizes the motions of the carriers in the z-direction together with the formation of the subband energies.

In Fig. 2.1a, the layers and the impurity types in different layers are shown. Electrons from neutral donors recombine with neutral acceptors, leaving behind a net space charge associated with ionized impurities. The concentration of the impurities is shown in Fig. 2.1b. The periodic potential is due to three terms:

$$V(z) = V_{\text{imp}}(z) + V_{\text{H}}(z) + V_{\text{xc}}(z),$$

where, $V_{\text{H}}(z)$is the Hartree potential of electrons and holes and $V_{\text{xc}}(z)$is the exchange potential. The potential due to ionized impurities, $V_{\text{imp}}(z)$is obtained from Poisson's equation:

S. Bhattacharya and K. P. Ghatak, *Effective Electron Mass in Low-Dimensional Semiconductors*, Springer Series in Materials Science 167,
DOI: 10.1007/978-3-642-31248-9_2, © Springer-Verlag Berlin Heidelberg 2013

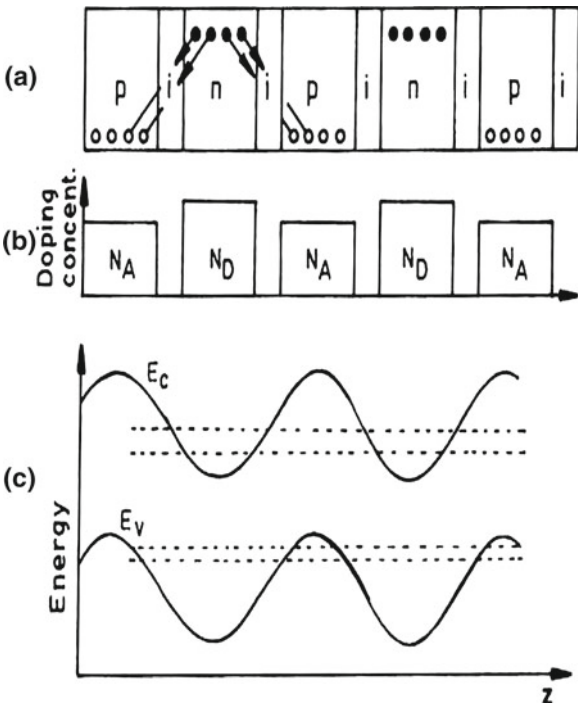

Fig. 2.1 Periodic band edge modulation in an NIPI SL: **a** structure; **b** doping profile; and **c** spatial variation of conduction and valence band edges showing the development of the 1D periodic potential

The Poisson's equation in this case is given by, [34]

$$\frac{\mathrm{d}^2 V_{\mathrm{imp}}}{\mathrm{d}z^2} = \frac{e^2}{\varepsilon_{\mathrm{sc}}}[N_{\mathrm{D}}(z) - N_{\mathrm{A}}(z)] \tag{2.1a}$$

where, $\varepsilon_{\mathrm{sc}}$ is the semiconductor permittivity,$N_{\mathrm{D}}(z)$is the donor concentration along z-axis and $N_{\mathrm{A}}(z)$is the acceptor concentration along z-axis.

Energy levels for the z quantized motion for electrons are to be calculated self-consistently from Schrodinger equation

$$\left[-\frac{\hbar^2}{2m_{\mathrm{e}}}\frac{\partial^2}{\partial z^2} + V(z)\right]\phi(z) = E\phi(z) \tag{2.1b}$$

where m_{e} is the effective electron mass, $\phi(z)$is the electron wave function, and E is the energy eigenvalue. The envelope function $\phi(z)$ is given by

$$\phi(z) = \sum_m \exp(iqmd)\, f(z - md) \tag{2.1c}$$

where d is the period.

Some special features of this SL are stated below [34]:

1. When there are equal numbers of donors and acceptors in a period, i.e.,

$$\int_{-d/2}^{d/2} N_{\mathrm{D}}(z)\mathrm{d}z = \int_{-d/2}^{d/2} N_{\mathrm{A}}(z)\mathrm{d}z \tag{2.1d}$$

there are no free carriers in the unexcited sample at low temperatures.

2. Assume that the thickness of the doping layers are equal: $d_n = d_p$, the doping levels are uniform: $N_{\mathrm{D}} = N_{\mathrm{A}}$, and also there is no undoped layer: $d_i = 0$. The periodic space charge layer is then due to impurity ions only. $V_{\mathrm{imp}}(z)$ is parabolic in nature and has amplitude

$$V_0 = \frac{e^2}{\varepsilon_s} N_{\mathrm{D}} d_n^2/8. \tag{2.1e}$$

The potential variation is sketched in Fig 2.1c. The effective energy gap becomes

$$E_{\mathrm{g}}(\mathrm{eff}) = E_{\mathrm{g}} - 2V_0 + E_{e0} + E_{h0} \tag{2.1f}$$

where, E_{e0} and E_{h0} are the energies of the first subbands. The envelope functions $\phi(z)$in the tight binding approximation are harmonic oscillator functions and the eigenvalues are expressed as

$$E_{\mathrm{en}} = \hbar \left(\frac{e^2 N_{\mathrm{D}}}{\varepsilon_{sc} m_e} \right)^{1/2} \left[n + 1/2 \right]. \tag{2.1g}$$

One may therefore conclude from (2.1g) and calculated values that the effective gap may be reduced from that in bulk material.

3. If the thickness of and/or the doping concentration in the n-layer is increased, there will be a finite, two-dimensional electron concentration in the n-layers. Therefore, it appears that the electronic structures of the nipi's differ radically from the corresponding bulk semiconductors as stated below:

   (a) Each band is split into mini bands.
   (b) The magnitude and spacing of these mini bands may be designed by the choice of the superlattices parameters and
   (c) The electron energy spectrum of the nipi crystal becomes two-dimensional leading to the step functional dependence of the density-of-states function.

In Sect. 2.2.1, of the theoretical background, the EEM in nipi structures of non-linear optical materials has been investigated. Section 2.2.2 contains the results for nipi structures of III–V, ternary and quaternary compounds in accordance with the three- and two-band models of Kane together with parabolic energy

bands and they form the special cases of Sect. 2.2.1. Sections 2.2.3–2.2.5 contain the study of the EEM for nipi's of II–VI, IV–VI, and stressed Kane-type semiconductors respectively. The Sect. 2.3 contains the results and discussion of this chapter. The last Sect. 2.4 presents the open research problems pertaining to this chapter.

2.2 Theoretical Background

2.2.1 Formulation of the EEM in Nipi Structures of Nonlinear Optical Materials

The dispersion relation of the conduction electrons in nipi structures of nonlinear optical materials can be expressed using (1.2) and following the method as given in [34, 35] as

$$\psi_1(E) = \psi_2(E)k_s^2 + \psi_3(E)\left(n_i + \frac{1}{2}\right)\frac{2m_{||}^*}{\hbar}\omega_8(E) \tag{2.1h}$$

where

$$\omega_8(E) \equiv \left(\frac{n_0\,|e|^2}{\varepsilon_{sc}\,[\theta_1(E)]}\right)^{1/2} \text{ and } \theta_1(E) \equiv \frac{\hbar^2}{2}\left\{\frac{\psi_3(E)\,[\psi_1(E)]' - \psi_1(E)\,[\psi_3(E)]'}{[\psi_3(E)]^2}\right\}$$

and $n_i (= 0, 1, 2\ldots)$ is the miniband index for nipi structures.

The EEM in this case assumes the form

$$m^*(E_{\mathrm{Fn}}, n_i) = \left(\frac{\hbar^2}{2}\right) R_{81}(E, n_i)\Big|_{E=\bar{E}_{\mathrm{Fn}}} \tag{2.2}$$

where,

$$\begin{aligned} R_{81}(E, n_i) \equiv [\psi_2(E)]^{-2}\Bigg[\psi_2(E)\Bigg\{[\psi_1(E)]' - \left(\frac{2m_{||}^*}{\hbar}\right)[\psi_3(E)]'\left(n_i + \frac{1}{2}\right)[\omega_8(E)] \\ - \left(\frac{2m_{||}^*}{\hbar}\right)[\psi_3(E)]\left(n_i + \frac{1}{2}\right)[\omega_8(E)]'\Bigg\} \\ - \left\{[\psi_1(E)] - \left(\frac{2m_{||}^*}{\hbar}\right)[\psi_3(E)]\left(n_i + \frac{1}{2}\right)[\omega_8(E)]\right\}[\psi_2(E)]'\Bigg] \end{aligned}$$

and $\bar{E}_{\mathrm{Fn}}$ is the Fermi energy in the present case as measured from the edge of the conduction band in vertically upward direction in the absence of any quantization.

From (2.2), we observe that the EEM is a function of the Fermi energy, nipi subband index, and the other material constants which is the characteristic feature of nipi structures of nonlinear optical materials.

The subband energy ($E_{1\mathrm{ni}}$) can be written as

$$\psi_1(E_{1\mathrm{ni}}) = \psi_3(E_{1\mathrm{ni}})\left(n_i + \frac{1}{2}\right)\frac{2m^*_{||}}{\hbar}\omega_8(E_{1\mathrm{ni}}) \tag{2.3}$$

The density-of-states function for nipi structures of non-linear optical materials can be expressed as

$$N_{\mathrm{nipi}}(E) = \frac{g_v}{2\pi d_0}\sum_{n_i=0}^{n_{i\,\max}} R_{81}(E, n_i)H(E - E_{1\mathrm{ni}}) \tag{2.4}$$

in which d_0 is the superlattice period.

The electron concentration, can be written as

$$n_0 = \frac{g_v}{2\pi d_0}\sum_{n_i=0}^{n_{i\,\max}}\left[T_{81}(\bar{E}_{\mathrm{Fn}}, n_i) + T_{82}(\bar{E}_{\mathrm{Fn}}, n_i)\right] \tag{2.5}$$

where, $T_{81}(\bar{E}_{\mathrm{Fn}}, n_i) \equiv \left[\psi_1(\bar{E}_{\mathrm{Fn}}) - \psi_3(\bar{E}_{\mathrm{Fn}})\left(n_i + \frac{1}{2}\right)\frac{2m^*_{||}}{\hbar}\omega_8(\bar{E}_{\mathrm{Fn}})\right]\left[\psi_2(\bar{E}_{\mathrm{Fn}})\right]^{-1}$

and $T_{82}(\bar{E}_{\mathrm{Fn}}, n_i) \equiv \sum_{r=1}^{s} L(r)T_{81}(\bar{E}_{\mathrm{Fn}}, n_i)$.

2.2.2 EEM in the Nipi Structures of III–V, Ternary and Quaternary Semiconductors

(a) The electron energy spectrum in nipi structures of III–V, ternary and quaternary materials can be expressed from (2.1) under the conditions $\Delta_{||} = \Delta_{\perp} = \Delta$, $\delta = 0$ and $m^*_{||} = m^*_{\perp} = m_c$, as

$$I_{11}(E) = \left(n_i + \frac{1}{2}\right)\hbar\omega_9(E) + \frac{\hbar^2 k_s^2}{2m_c} \tag{2.6}$$

where $\omega_9(E) \equiv \left(\frac{n_0\,|e|^2}{\varepsilon_{\mathrm{sc}} I'(E) m_c}\right)^{1/2}$.

The EEM in this case can be written as

$$m^*(E_{\mathrm{Fn}}, n_i) = m_c R_{82}(E, n_i)|_{E=E_{\mathrm{Fn}}} \tag{2.7}$$

in which, $R_{82}(E, n_i) \equiv \left\{[I_{11}(E)]' - \left(n_i + \frac{1}{2}\right)\hbar\,[\omega_9(E)]'\right\}$.
From (2.7) we observe that the EEM in this case is a function of the Fermi energy, nipi subband index and the other material constants which is the characteristic feature of nipi structures of III–V, ternary and quaternary compounds whose bulk dispersion relations is defined by the three-band model of Kane.
The subband energies ($E_{2\mathrm{ni}}$)can be written as

$$I_{11}(E_{2\mathrm{ni}}) = \left(n_i + \frac{1}{2}\right)\hbar\omega_9(E_{2\mathrm{ni}}). \tag{2.8}$$

The density-of-states function in this case can be expressed as

$$N_{\mathrm{nipi}}(E) = \frac{m_c g_v}{\pi\hbar^2 d_0}\sum_{n_i=0}^{n_{i\,\max}} R_{82}(E, n_i)H(E - E_{2\mathrm{ni}}). \tag{2.9}$$

The use of (2.9) leads to the expression of the electron concentration as

$$n_0 = \frac{m_c g_v}{\pi\hbar^2 d_0}\sum_{n_i=0}^{n_{i\,\max}}\left[T_{83}(\bar{E}_{\mathrm{Fn}}, n_i) + T_{84}(\bar{E}_{\mathrm{Fn}}, n_i)\right] \tag{2.10}$$

where $T_{83}(\bar{E}_{\mathrm{Fn}}, n_i) \equiv \left[I_{11}(\bar{E}_{\mathrm{Fn}}) - \left(n_i + \frac{1}{2}\right)\hbar\omega_9(\bar{E}_{\mathrm{Fn}})\right]$ and $T_{84}(\bar{E}_{\mathrm{Fn}}, n_i) \equiv \sum_{r=1}^{s} L(r)T_{83}(\bar{E}_{\mathrm{Fn}}, n_i)$.

(b) For the two-band model of Kane, the expressions of the dispersion relation, the EEM, the subband energies, the density-of-states function, and n_0 remain the same where

$$I_{11}(E) = E(1 + \alpha E), \quad \{I_{11}(E)\}' = (1 + 2\alpha E) \quad \text{and} \quad \{I_{11}(E)\}'' = 2\alpha.$$

The EEM in this case can be written as

$$m^*(E_{\mathrm{Fn}}, n_i) = m_c\left\{(1 + 2\alpha E_{\mathrm{Fn}}) + \left(n_i + \frac{1}{2}\right)\hbar\,[\omega_9(E_{\mathrm{Fn}})]\,\frac{\alpha}{(1 + 2\alpha E_{\mathrm{Fn}})}\right\} \tag{2.11}$$

From 2.11 we observe that the EEM in this case is a function of the Fermi energy, nipi subband index and the other material constants due to the band nonparabolicity only.

(c) For parabolic energy bands, the forms of the expressions of dispersion relation, the EEM, the subband energies, the density-of-states function ,and n_0 remain the same, where $I_{11}(E) = E$,

$$\{I_{11}(E)\}' = 1 \quad \text{and} \quad \{I_{11}(E)\}'' = 0.$$

The EEM can be written as

$$m^*(E_{\mathrm{Fn}}, n_i) = m_c. \tag{2.12}$$

From (2.12) we observe that the EEM in this case is a constant quantity.

2.2.3 EEM in the Nipi Structures of II–VI Semiconductors

The carrier dispersion law in nipi structures of II–VI compounds can be expressed as

$$E = a_0' k_s^2 + \left(n_i + \frac{1}{2}\right)\hbar\omega_{10} \pm \bar{\lambda}_0 k_s, \quad \omega_{10} \equiv \left(\frac{n_0 |e|^2}{\varepsilon_{sc} m_{||}^*}\right)^{1/2}. \tag{2.13}$$

Using (2.13), the EEM in this case can be written as

$$m^*(E_{\mathrm{Fn}}, n_i) = m_{\perp}^* \left\{1 - \bar{\lambda}_0 \left[(\bar{\lambda}_0)^2 + 4a_0' E_{\mathrm{Fn}} - 4a_0'\left(n_i + \frac{1}{2}\right)\hbar\omega_{10}\right]^{-1/2}\right\}. \tag{2.14}$$

Thus, the EEM in this case is a function of the Fermi energy, the nipi subband index number and the energy spectrum constants due to the presence of only $\bar{\lambda}_0$.

The subband energies ($E_{3\mathrm{ni}}$)can be written as

$$E_{3\mathrm{ni}} = \left(n_i + \frac{1}{2}\right)\hbar\omega_{10} \tag{2.15}$$

The density-of-states function in this case can be expressed as

$$N_{\mathrm{nipi}}(E) = \frac{m_{\perp}^* g_v}{\pi\hbar^2 d_0} \sum_{n_i=0}^{n_{i\,\max}} \left[1 - \frac{a_{81}}{\sqrt{E + b_{81}(n_i)}}\right] H(E - E_{3\mathrm{ni}}) \tag{2.16}$$

in which, $a_{81} \equiv \frac{\bar{\lambda}_0}{2\sqrt{a_0'}}$ and $b_{81}(n_i) \equiv \left[\frac{1}{4a_0'}\left[(\bar{\lambda}_0)^2 - 4a_0'\left(n_i + \frac{1}{2}\right)\hbar\omega_{10}\right]\right]$.

The use of the (2.16) leads to the electron concentration under the condition of extreme degeneracy as

$$n_0 = \frac{g_v m_{\perp}^*}{\pi\hbar^2} \sum_{ni=0}^{ni_{\max}} \left(E_{\mathrm{Fn}} - E_{3\mathrm{ni}} + (\overline{\lambda_0})^2 m_{\perp}^* \hbar^{-2}\right) \tag{2.17}$$

2.2.4 EEM in the Nipi Structures of IV–VI Semiconductors

The carrier energy spectrum in nipi structures of IV–VI compounds can be written as

$$k_s^2 = (\hbar^2 S_{19})^{-1}\left[-S_{20}(E,n_i) + \sqrt{S_{20}^2(E,n_i) + 4S_{19}S_{21}(E,n_i)}\right] \tag{2.18}$$

in which,

$$S_{19} \equiv (\frac{\alpha}{m_t^+ m_t^-}), \quad S_{20}(E,n_i) \equiv \left\{\frac{1}{m_t^*} - \left(\frac{\alpha E}{m_t^+}\right) + \frac{1+\alpha E}{m_t^-} + \frac{\alpha\hbar^2}{2m_l^+ m_t^-}\left(n_i + \frac{1}{2}\right) T(E) + \frac{\alpha\hbar^2}{2m_l^- m_t^+}\left(n_i + \frac{1}{2}\right) T(E)\right\}$$

$$T(E) \equiv \frac{2m^*(0)}{\hbar}\omega_{11}(E),\ m^*(0) \equiv \left(\frac{m_l^* m_l^-}{m_l^* + m_l^-}\right), \quad \omega_{11}(E) \equiv \left(\frac{n_0\,|e|^2}{\varepsilon_{sc} m^*(E)}\right)^{1/2},$$

$$m^*(E) \equiv \frac{1}{4t_1}\left[-(t_2(E))' + \frac{t_2(E)(t_2(E))' + 2t_1(1+2\alpha E)}{\sqrt{t_2^2(E) + 4Et_1(1+\alpha E)}}\right],$$

$$t_1 \equiv \left(\frac{\alpha}{4m_l^+ m_l^-}\right), \quad t_2(E) \equiv \frac{1}{2}\left[\left(\frac{1}{m_l^*}\right) - \left(\frac{\alpha E}{m_l^+}\right) + \left(\frac{1+\alpha E}{m_l^-}\right)\right],$$

$$(t_2(E))' \equiv \frac{\alpha}{2}\left(\frac{1}{m_l^-} - \left(\frac{1}{m_l^+}\right)\right) \text{ and}$$

$$S_{21}(E,n_i) \equiv \left[E(1+\alpha E) + \frac{\alpha E\hbar^2}{2m_l^+}\left(n_i + \frac{1}{2}\right) T(E) + \frac{\hbar^2}{2m_l^-}\left(n_i + \frac{1}{2}\right) T(E)(1+\alpha E) + \frac{\hbar^4}{4m_l^- m_l^+}\left(n_i + \frac{1}{2}\right) T(E) - \left(\frac{\hbar^2}{2m_l^*}\right) T(E)\left(n_i + \frac{1}{2}\right)\right].$$

Using (2.18), the EEM in this case can be written as

$$m^*(E_{\mathrm{Fn}}, n_i) = R_{84}(E,n_i)|_{E=E_{\mathrm{Fn}}} \tag{2.19}$$

where,

$$R_{84}(E,n_i) \equiv (2S_{19})^{-1} \times \left[-(S_{20}(E,n_i))' + \frac{S_{20}(E,n_i)\left[S_{20}(E,n_i)\right]' + 2S_{19}\left[S_{21}(E,n_i)\right]'}{\left[\left\{\left[S_{20}(E,n_i)\right]'\right\}^2 + 4S_{19}S_{21}(E,n_i)\right]^{1/2}} \right].$$

Thus, one can observe that the EEM in this case is a function of both the Fermi energy and the nipi subband index number together with the spectrum constants of the system due to the presence of band nonparabolicity.

The subband energies ($E_{4\mathrm{ni}}$) can be written as

$$\left[E_{4\mathrm{ni}} - \frac{\hbar^2}{2m_l^-}T(E_{4\mathrm{ni}})\left(n_i + \frac{1}{2}\right)\right] \times \left[1 + \alpha E_{4\mathrm{ni}} + +\alpha\frac{\hbar^2}{2m_l^+}T(E_{4\mathrm{ni}})\left(n_i + \frac{1}{2}\right)\right] = \left[\frac{\hbar^2}{2m_l^*}T(E_{4\mathrm{ni}})\left(n_i + \frac{1}{2}\right)\right]. \tag{2.20}$$

The density-of-states function in this case assumes the form as

$$N_{\mathrm{nipi}}(E) = \frac{g_v}{\pi\hbar^2 d_0}\sum_{n_i=0}^{n_{i\,\max}} R_{84}(E,n_i)H(E - E_{4\mathrm{ni}}) \tag{2.21}$$

The use of (2.21) leads to the expression of the electron concentration as

$$n_0 = \frac{g_v}{2\pi\hbar^2 S_{19}d_0}\sum_{n_i=0}^{n_{i\,\max}}\left[T_{85}(\bar{E}_{\mathrm{Fn}},n_i) + T_{86}(\bar{E}_{Fn},n_i)\right] \tag{2.22}$$

where, $T_{85}(\bar{E}_{\mathrm{Fn}},n_i) \equiv \left[-S_{20}(E_{\mathrm{Fn}},n_i) + \sqrt{[S_{20}(E_{\mathrm{Fn}},n_i)]^2 + 4S_{19}S_{21}(E_{\mathrm{Fn}},n_i)}\right]$ and $T_{86}(\bar{E}_{\mathrm{Fn}},n_i) \equiv \sum_{r=1}^{s} L(r)T_{85}(\bar{E}_{\mathrm{Fn}},n_i)$.

2.2.5 EEM in the Nipi Structures of Stressed Semiconductors

The electron dispersion law in the nipi structures of stressed semiconductors can be written as

$$\frac{k_x^2}{[\bar{a}_0(E)]^2}+\frac{k_y^2}{[\bar{b}_0(E)]^2}+\frac{1}{[\bar{c}_0(E)]^2}\frac{2m_z^*(0)}{\hbar}\left(n_i+\frac{1}{2}\right)\omega_{12}(E)=1 \tag{2.23}$$

where $\omega_{12}(E)\equiv\left(\frac{n_0|e|^2}{\varepsilon_{sc}m_z^*(E)}\right)^{1/2}$ and $m_z^*(E)\equiv\hbar^2\bar{c}_0(E)\frac{\partial}{\partial E}[\bar{c}_0(E)]$.

The use of (2.23) leads to the expression of the EEM as

$$m^*(E_{Fn},n_i)=\left(\frac{\hbar^2}{2}\right)R_{85}(E,n_i)\Big|_{E=E_{Fn}} \tag{2.24}$$

where,

$$\begin{aligned}R_{85}(E,n_i)\equiv&\left[\left[(\bar{a}_0(E))'b_0(E)+(\bar{b}_0(E))'\bar{a}_0(E)\right]\right.\\&\times\left[1-\frac{1}{[\bar{c}_0(E)]^2}\frac{2m_z^*(0)}{\hbar}\left(n_i+\frac{1}{2}\right)\omega_{12}(E)\right]\\&-\left[\frac{\bar{a}_0(E)\bar{b}_0(E)}{[\bar{c}_0(E)]^2}\frac{2m_z^*(0)}{\hbar}\left(n_i+\frac{1}{2}\right)[\omega_{12}(E)]'\right]\\&\left.+\left[\frac{\bar{a}_0(E)\bar{b}_0(E)[\bar{c}_0(E)]'}{[\bar{c}_0(E)]^3}\frac{4m_z^*(0)}{\hbar}\left(n_i+\frac{1}{2}\right)[\omega_{12}(E)]\right]\right].\end{aligned}$$

Thus, the EEM is a function of the Fermi energy and the nipi subband index due to the presence of stress and band nonparabolicity only.

The subband energies (E_{5ni})can be written as

$$\frac{1}{[\bar{c}_0(E_{4\mathrm{ni}})]^2}\frac{2m_z^*(0)}{\hbar}\left(n_i+\frac{1}{2}\right)\omega_{12}(E_{4\mathrm{ni}})=1. \tag{2.25}$$

The density-of-states function can be expressed as

$$N_{\mathrm{nipi}}(E)=\frac{g_v}{\pi\hbar^2d_0}\sum_{n_i=0}^{n_{i\,\max}}R_{85}(E,n_i)H(E-E_{5\mathrm{ni}}). \tag{2.26}$$

Thus, using (2.26), the electron concentration in nipi structures of stressed compounds can be written as

$$n_0=\frac{g_v}{2\pi d_0}\sum_{n_i=0}^{n_{i\,\max}}\left[C_3(\bar{E}_{\mathrm{Fn}},n_i)+C_4(\bar{E}_{\mathrm{Fn}},n_i)\right]. \tag{2.27}$$

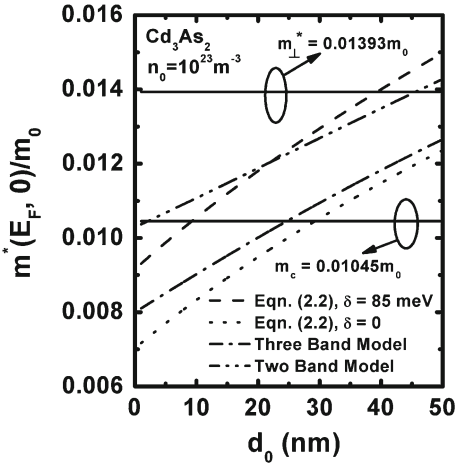

Fig. 2.2 Plot of the EEM as function of superlattice period for n-Cd_3As_2 considering Eq. (2.2) The plots for three- and two-band models of Kane have also been exhibited with their corresponding bulk values

where

$$C_3(\bar{E}_{\mathrm{Fn}}, n_i) \equiv \bar{a}_0(\bar{E}_{\mathrm{Fn}})\bar{b}_0(E_{\mathrm{Fn}})\left[1 - \frac{2m_z^*(0)}{\hbar}\left(n_i + \frac{1}{2}\right)\frac{\omega_{12}(\bar{E}_{\mathrm{Fn}})}{(\bar{c}_0(\bar{E}_{\mathrm{Fn}}))^2}\right]$$

and

$$C_4(\bar{E}_{\mathrm{Fn}}, n_i) \equiv \sum_{r=1}^{s} L(r)C_3(\bar{E}_{\mathrm{Fn}}, n_i).$$

2.3 Results and Discussion

The effect of nipi superlattice period on the EEM has been exhibited in Figs. 2.2, 2.3, 2.4, 2.5, 2.6, 2.7, 2.8, 2.9, 2.10 for different materials. Using (2.2) and (2.5) together with the energy band constants as given in Table 1.1, we have plotted the EEM in nipi structures of nonlinear optical materials taking Cd_3As_2 and $CdGeAs_2$ as examples in Figs. 2.2 and 2.3

From both Figs. 2.2 and 2.3, it appears that the effect of increment of the superlattice period increases the EEM in the presence of extreme carrier degeneracy of the order of 10^{23} m^{-3}. For comparison with the bulk anisotropic effective masses, we have also exhibited the same in the said figures. It appears that the EEM can be much less than that of the corresponding bulk values below 10 nm period for Cd_3As_2. Thus in such condition, one can expect an increase in the carrier mobility to a great extent,

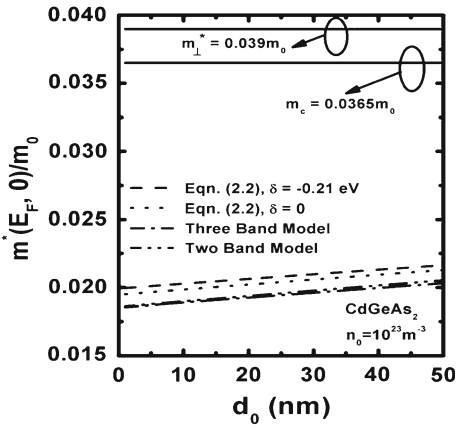

Fig. 2.3 Plot of the EEM as function of superlattice period for n-$CdGeAs_2$ for all cases of Fig. 2.2

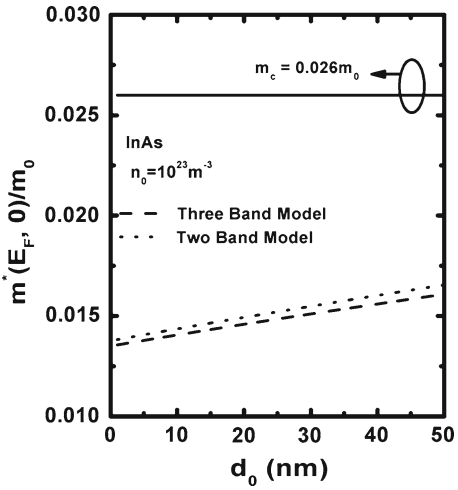

Fig. 2.4 Plot of the EEM as function of superlattice period for n-InAs considering the three- and two-band model of Kane with the corresponding bulk value

in fact almost double. The effect of crystal field splitting has also been exhibited in the same Figs. 2.2 and 2.3.

It appears that the effect of δ on the EEM is the largest in case of Cd_3As_2. The approximation in the energy band structure also makes a significant deviation of the EEM in case of Cd_3As_2. However, for $CdGeAs_2$, the EEM exhibits a slow variation over the superlattice period as compared with Fig. 2.2 At this point it should be noted that with the increase in the superlattice period, the EEM in Cd_3As_2 by considering the energy dispersion relation with the absence of the crystal field splitting and the three-band model of Kane actually tends to the anisotropic bulk value $0.01393m_0$.

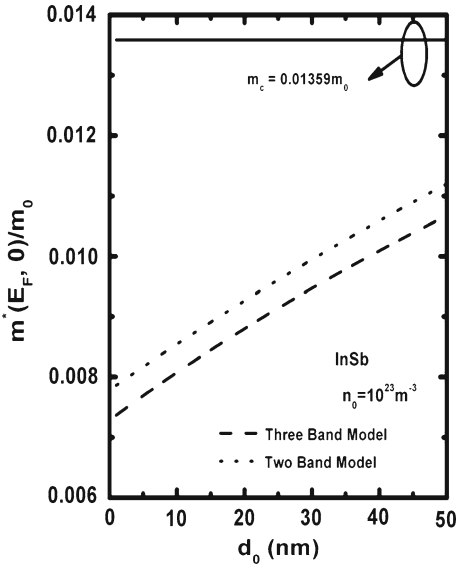

Fig. 2.5 Plot of the EEM as function of superlattice period for n-InSb considering the three- and two-band model of Kane with the corresponding bulk value

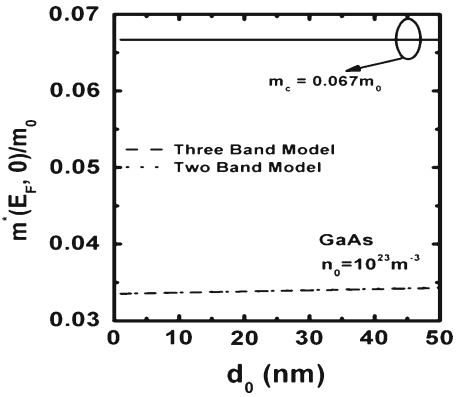

Fig. 2.6 Plot of the EEM as function of superlattice period for n-GaAs considering the three- and two-band model of Kane with the corresponding bulk value

This is not with the case when the effect of crystal field splitting and the two-band equivalent model is considered. In these two cases, the EEM is overestimated against the bulk value. This is not with the case of Fig. 2.3 of $CdGeAs_2$, where the EEM converges to the bulk anisotropic value at larger superlattice period.

The effect of superlattice period on the EEM in the ground state subband in III–V materials has been evaluated using the three- and the two-band model of Kane in Figs. 2.4, 2.5, 2.6 for InAs, InSb and GaAs respectively.

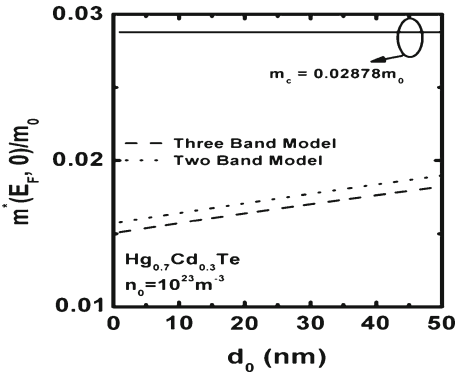

Fig. 2.7 Plot of the EEM as function of superlattice period for n-$Hg_{1-x}Cd_xTe$ considering the three- and two-band model of Kane with the corresponding bulk value at $x = 0.3$

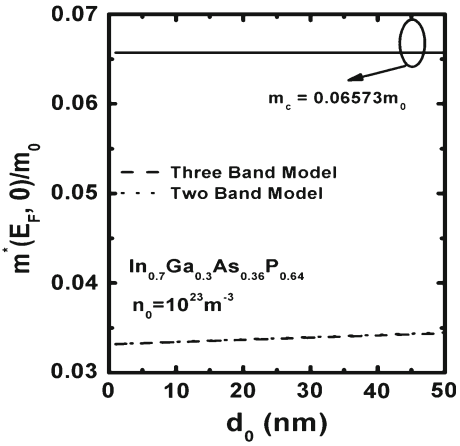

Fig. 2.8 Plot of the EEM as function of superlattice period for n-$In_{1-x}Ga_xAs_{1-y}P_y$ considering the three- and two-band model of Kane with the corresponding bulk value at $x = 0.3$

It appears from these figures that the effect of the variation of the energy dispersion relation model on EEM is almost insignificant for GaAs nipi structures, whereas for InSb, the EEM exhibits a significant deviation. In almost all the cases of about 1 nm period, the EEM approximately becomes half of the respective isotropic effective bulk masses indicating the mobility rise of up to 200 %.

In Figs. 2.7 and 2.8, the EEM as function of the periods has been further evaluated for the ternary and quaternary materials like $Hg_{1-x}Cd_xTe$ and $In_{1-x}Ga_xAs_{1-y}P_y$, where the energy band gap in these materials can be modulated by changing the alloy fraction x. We see that the EEM in case of $In_{1-x}Ga_xAs_{1-y}P_y$ almost exhibits no significant variation and approaches quickly its bulk normalized value 0.0287 at $x = 0.3$ as compared to $Hg_{1-x}Cd_xTe$.

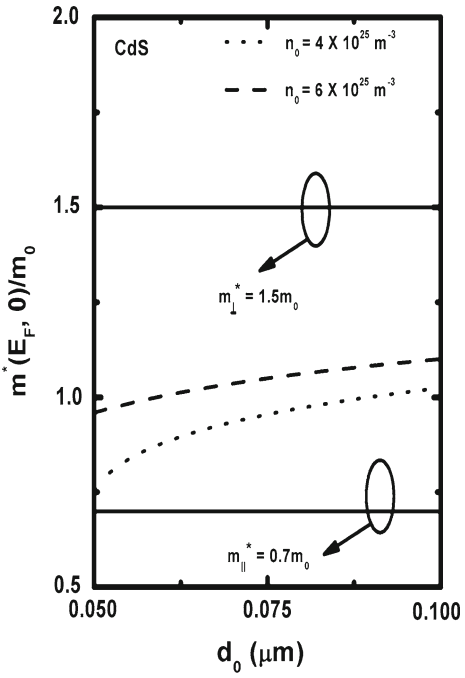

Fig. 2.9 Plot of the EEM as function of superlattice period for p-CdS

Figures 2.9 and 2.10 exhibit the EEM at the lowest subband in II–VI and IV–VI nipi structures of CdS and PbTe respectively.

The effect of increasing the doping concentration from 4×10^{25} to 6×10^{25} m^{-3} on EEM in CdS has been also exhibited in Fig. 2.9 for a period bandwidth of $50-100$ μm. It appears that with the increase in the doping concentration, the EEM in CdS increases and approaches the bulk longitudinal normalized value 1.5. However, in case of PbTe, we see that the EEM saturates above superlattice period of about 20 μm.

The effect of doping concentration on the EEM in the lowest subband level in all the aforementioned materials has been exhibited in Figs. 2.11, 2.12, 2.13, 2.14, 2.15, 2.16, 2.17, 2.18. It appears that the EEM increases with the increases in carrier degeneracy for all the cases and may become even larger than that of their corresponding bulk value along the proper transport direction. From Fig. 2.12 we see that the EEM is almost constant below the degeneracy of about 10^{23} m^{-3}. The effect of different models of energy band structures has been exhibited to present the dependency of the EEM on the same. It appears from Figs. 2.15 and 2.17 that the second and third order Kane model almost exhibits no differences of the EEM from the two. The respective saturation of the EEM with the decrease in the degeneracy is different for the materials as this depends on the Fermi energy which is a function of the energy band parameters.

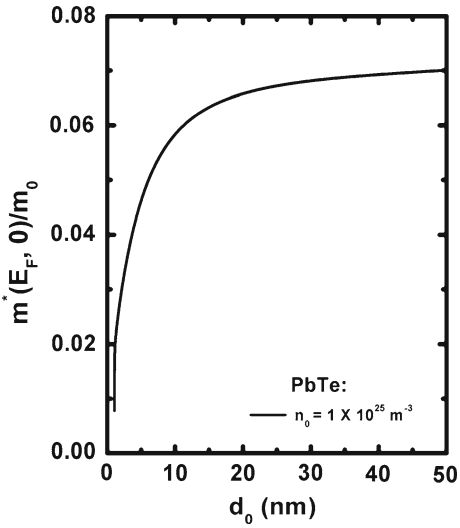

Fig. 2.10 Plot of the EEM as function of superlattice period for PbTe

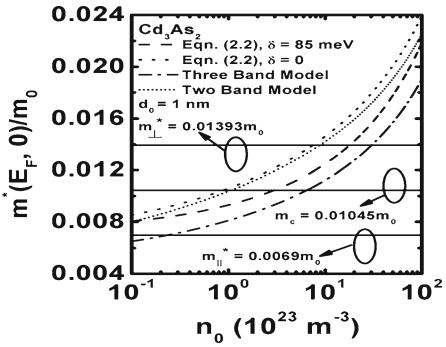

Fig. 2.11 Plot of the EEM as function of doping concentration for n-Cd_3As_2 considering all cases of Fig. 2.2

Figure 2.18 exhibits the variation of the EEM with increasing degeneracy for PbTe nipi. Anomalous behavior in the variation of the EEM has been exhibited as one increases the degeneracy. It appears that above 2×10^{22} m^{-3}, the EEM decreases. This should not be in general confused with other plots since an increase in the degeneracy increases the Fermi energy which increases the EEM. However, in this case, the effect of the different spectrum constants defines the variation of the EEM.

The variation of the EEM with alloy composition for the ternary and quaternary materials has been exhibited in Fig. 2.19 for the three- and two-energy band model of Kane. Almost no difference in the two-energy band model in this case is exhibited. The variation of the EEM for the quaternary is slower than that of the ternary which is due to the variation of the energy band gap through the alloy composition. The

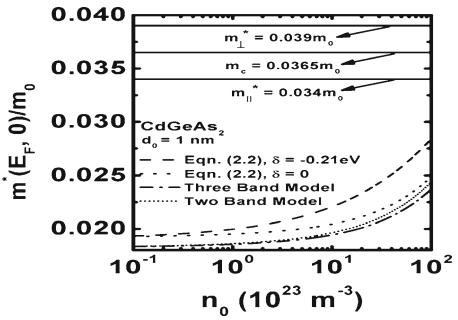

Fig. 2.12 Plot of the EEM as function of doping concentration for n-$CdGeAs_2$ considering all cases of Fig. 2.3

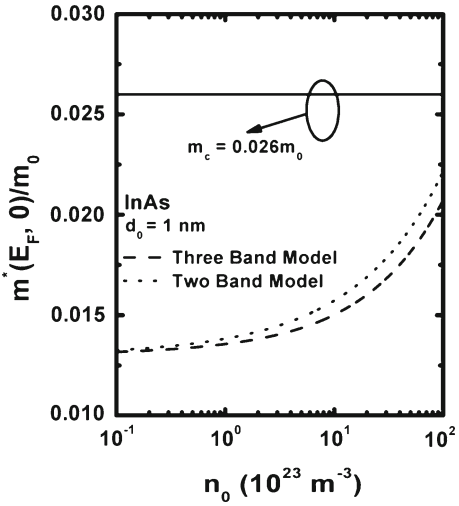

Fig. 2.13 Plot of the EEM as function of doping concentration for n-InAs considering all cases of Fig. 2.4

joy of executing the intricate computer programming for the variation of EEM in case of stressed InSb nipi structure whose energy band parameters have been given in Table 1.1 of Chap. 1 has been left to the reader. The summary of this chapter is presented in Table 2.1.

2.4 Open Research Problems

R.2.1 Investigate the EEM, EAM, DEM, CEM, CoEM, FREM, and OEM in the presence of an arbitrarily oriented nonquantizing magnetic field for nipi

Table 2.1 The electron statistics and the EEM in the nipi structures of nonlinear optical, III–V, ternary, quaternary, II–VI, IV–VI and stressed materials

Type of materials	The EEM	The electron statistics
1. Non-linear optical semiconductors	$m^*(E_{\mathrm{Fn}}, n_i) = \left(\frac{\hbar^2}{2}\right) R_{81}(E, n_i)\Big\vert_{E=\bar{E}_{\mathrm{Fn}}}$ (2.2)	$n_0 = \frac{g_v}{2\pi d_0} \sum_{n_i=0}^{n_i\,\max} \left[T_{81}(\bar{E}_{\mathrm{Fn}}, n_i) + T_{82}(\bar{E}_{\mathrm{Fn}}, n_i)\right]$ (2.5)
2. III–V semiconductors		
i. (a) Three band model of Kane	$m^*(E_{\mathrm{Fn}}, n_i) = m_c R_{82}(E, n_i)\vert_{E=E_{\mathrm{Fn}}}$ (2.7)	$n_0 = \frac{m_c g_v}{\pi \hbar^2 d_0} \sum_{n_i=0}^{n_i\,\max} \left[T_{83}(\bar{E}_{\mathrm{Fn}}, n_i) + T_{84}(\bar{E}_{\mathrm{Fn}}, n_i)\right]$ (2.10)
(b) Two band model of Kane	$m^*(E_{\mathrm{Fn}}, n_i) = m_c \left\{(1 + 2\alpha E_{\mathrm{Fn}}) + \left(n_i + \frac{1}{2}\right) \times \hbar\left[\omega_9(E_{Fn})\right] \frac{\alpha}{(1 + 2\alpha E_{Fn})}\right\}$ (2.11)	(2.10) remains same where $I(E) = E(1 + \alpha E)$, $\{I(E)\}' = (1 + 2\alpha E)$ and $\{I(E)\}'' = 2\alpha$
3. II–VI semiconductors	$m^*(E_{\mathrm{Fn}}, n_i) = m_\perp^* \left\{1 - \bar{\lambda}_0[(\bar{\lambda}_0)^2 + 4a_0' E_{\mathrm{Fn}} - 4a_0' \left(n_i + \frac{1}{2}\right) \hbar\omega_{10}]^{-1/2}\right\}$ (2.14)	$n_0 = \frac{g_v m_\perp^*}{\pi \hbar^2} \sum_{ni=0}^{ni_{\max}} \left(E_{\mathrm{Fn}} - E_{3ni} + (\overline{\lambda_0})^2 m_\perp^* \hbar^{-2}\right)$ (2.17)
4. IV–VI semiconductors	$m^*(E_{\mathrm{Fn}}, n_i) = R_{84}(E, n_i)\vert_{E=E_{\mathrm{Fn}}}$ (2.19)	$n_0 = \frac{g_v}{2\pi \hbar^2 S_{19} d_0} \sum_{n_i=0}^{n_i\,\max} \left[T_{85}(\bar{E}_{\mathrm{Fn}}, n_i) + T_{86}(\bar{E}_{\mathrm{Fn}}, n_i)\right]$ (2.22)
5. Stressed materials	$m^*(E_{\mathrm{Fn}}, n_i) = \left(\frac{\hbar^2}{2}\right) R_{85}(E, n_i)\Big\vert_{E=E_{\mathrm{Fn}}}$ (2.24)	$n_0 = \frac{g_v}{2\pi d_0} \sum_{n_i=0}^{n_i\,\max} \left[C_3(\bar{E}_{\mathrm{Fn}}, n_i) + C_4(\bar{E}_{\mathrm{Fn}}, n_i)\right]$ (2.27)

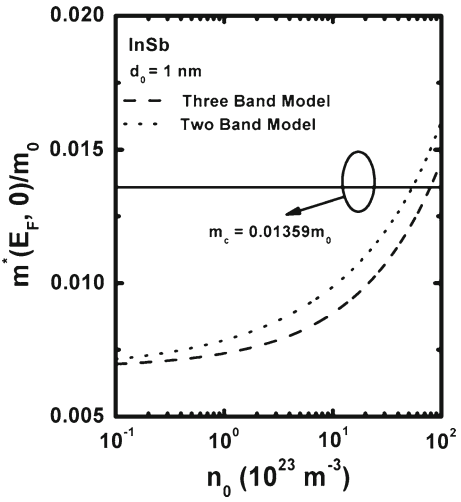

Fig. 2.14 Plot of the EEM as function of doping concentration for n-InSb considering all cases of Fig. 2.5

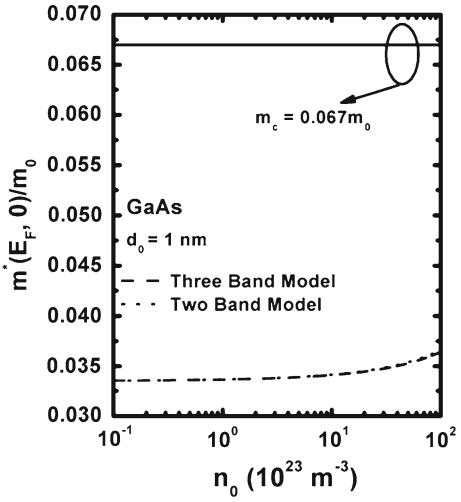

Fig. 2.15 Plot of the EEM as function of doping concentration for n-GaAs considering all cases of Fig. 2.6

structures of nonlinear optical semiconductors by including the electron spin. Study all the special cases for III–V, ternary and quaternary materials in this context.

R.2.2 Investigate the same set of masses as defined in (R 2.1) in nipi structures of IV–VI, II–VI and stressed Kane-type compounds in the presence of an

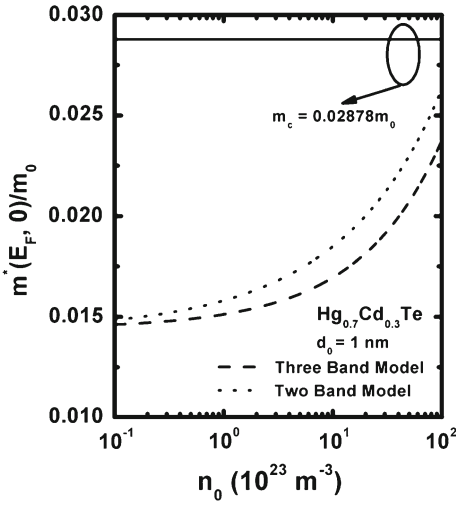

Fig. 2.16 Plot of the EEM as function of doping concentration for n-$Hg_{1-x}Cd_xTe$ considering all cases of Fig. 2.7

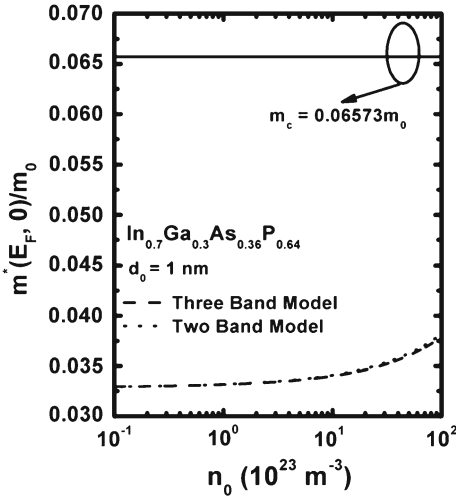

Fig. 2.17 Plot of the effective electron mass as function of doping concentration for n-$In_{1-x}Ga_xAs_{1-y}P_y$

arbitrarily oriented nonquantizing magnetic field by including the electron spin.

R.2.3 Investigate the same set of masses as defined in (R 2.1) for nipi structures of all the materials as stated in R.1.1 of chapter 1.

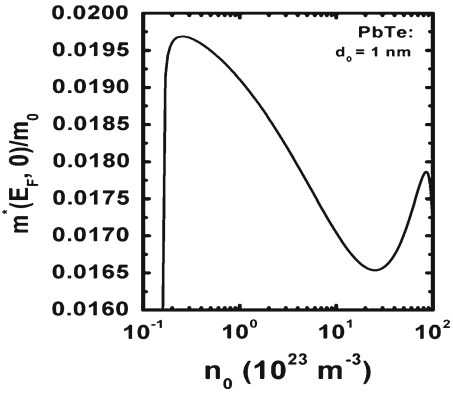

Fig. 2.18 Plot of the effective electron mass as function of doping concentration for PbTe

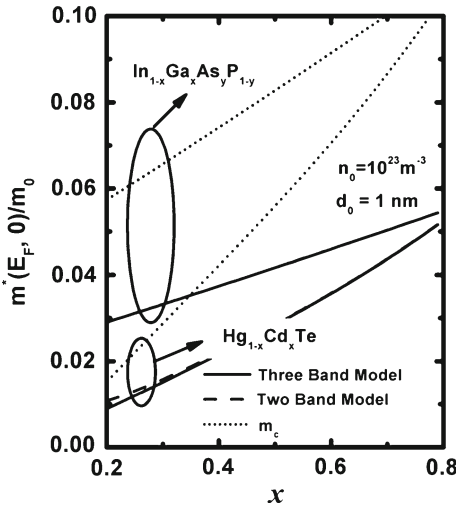

Fig. 2.19 Plot of the EEM as function of alloy composition for $Hg_{1-x}Cd_xTe$ and n-$In_{1-x}Ga_xAs_{1-y}P_y$ considering the three- and two-band model of Kane with the corresponding bulk value at different x

R.2.4 Investigate the same set of masses as defined in (R 2.1) for all the problems from R.2.1 to R.2.3 in the presence of an additional arbitrarily oriented electric field.

R.2.5 Investigate the same set of masses as defined in (R 2.1) for all the problems from R.2.1 to R.2.3 in the presence of arbitrarily oriented crossed electric and magnetic fields.

R 2.6 Investigate the same set of masses as defined in (R 2.1) for nipi structures of the heavily doped semiconductors in the presences of Gaussian, exponential, Kane, Halperian, Lax, and Bonch-Burevich types of Band tails for all

systems whose unperturbed carrier energy spectra are defined in R1.1 and R1.2 respectively.

R 2.7 Investigate the same set of masses as defined in (R 2.1) for nipi structures of the negative refractive index, organic, magnetic, and other advanced optical materials in the presence of an arbitrarily oriented alternating electric field.

R 2.8 Investigate the same set of masses as defined in (R 2.1) for all the nipi systems of this chapter in the presence of finite potential wells.

R 2.9 Investigate the same set of masses as defined in (R 2.1) for all the nipi systems of this chapter in the presence of parabolic potential wells.

R 2.10 Investigate all the appropriate problems of this chapter by including the many body, image force, broadening, and hot carrier effects respectively.

R 2.11 Investigate all the appropriate problems of this chapter by removing all the mathematical approximations and establishing the respective appropriate uniqueness conditions.

References

1. L. Esaki, R. Tsu, IBM J. Res. Dev. **14**, 61 (1970)
2. G.H. Döhler, Phys. Status Solidi B **52**, 79 (1972)
3. G.H. Döhler, Phys. Status Solidi B **52**, 533 (1972)
4. G.H. Döhler, Surf. Sci. **73**, 97 (1978)
5. G.H. Döhler, J. Vac. Sci. Technol. **16**, 851 (1979)
6. G.H. Döhler, K. Ploog, Prog. Cryst. Growth Charact. **2**, 145 (1979)
7. G.H. Döhler, H. Künzel, K. Ploog, Phys. Rev. B **25**, 2616 (1982)
8. H. Künzel, G.H. Döhler, A. Fischer, K. Ploog, Appl. Phys. Lett. **38**, 171 (1980)
9. G.H. Döhler, H. Künzel, D. Olego, K. Ploog, P. Ruden, H.J. Stolz, Phys. Rev. Lett. **47**, 864 (1981)
10. K. Ploog, H. Künzel, J. Knecht, A. Fischer, G.H. Döhler, Appl. Phys. Lett. **38**, 870 (1981)
11. K. Ploog, A. Fischer, H. Künzel, J. Electrochem. Soc. **128**, 400 (1981)
12. H. Jung, G.H. Döhler, H. Kunzel, K. Ploog, P. Ruden, H.J. Stolz, Solid State Commun. **43**, 291 (1982)
13. H. Künzel, G.H. Döhler, P. Ruden, K. Ploog, Appl. Phys. Lett. **41**, 852 (1982)
14. N.G. Anderson, W.D. Laidig, R.M. Kolbas, Y.C. Lo, J. Appl. Phys. **60**, 2361 (1986)
15. F. Capasso, Semiconduct. Semimet. **22**, 2 (1985)
16. F. Capasso, K. Mohammed, A.Y. Cho, R. Hull, A.L. Hutchinson, Appl. Phys. Lett. **47**, 420 (1985)
17. F. Capasso, R.A. Kiehl, J. Appl. Phys. **58**, 1366 (1985)
18. K. Ploog, G.H. Doheler, Adv. Phys. **32**, 285 (1983)
19. F. Capasso, K. Mohammed, A.Y. Cho, Appl. Phys. Lett. **478**, (1986)
20. R. Grill, C. Metzner, G.H. Döhler, Phys. Rev. B **63**, 235316 (2001)
21. J.Z. Wang, Z.G. Wang, Z.M. Wang, S.L. Feng, Z. Yang, Phys. Rev. B **62**, 6956 (2000)
22. J.Z. Wang, Z.G. Wang, Z.M. Wang, S.L. Feng, Z. Yang, Phys. Rev. B **61**, 15614 (2000)
23. A.R. Kost, M.H. Jupina, T.C. Hasenberg, E.M. Garmire, J. Appl. Phys. **99**, 023501 (2006)
24. A.G. Smirnov, D.V. Ushakov, V.K. Kononenko, Proc. SPIE **4706**, 70 (2002)
25. D.V. Ushakov, V.K. Kononenko, I.S. Manak, Proc. SPIE **4358**, 171 (2001)
26. J.Z. Wang, Z.G. Wang, Z.M. Wang, S.L. Feng, Z. Yang, Phys. Rev. B **62**, 6956 (2000)
27. A.R. Kost, L. West, T.C. Hasenberg, J.O. White, M. Matloubian, G.C. Valley, Appl. Phys. Lett. **63**, 3494 (1993)

28. S. Bastola, S.J. Chua, S.J. Xu, J. Appl. Phys. **83**, 1476 (1998)
29. Z.J. Yang, E.M. Garmire, D. Doctor, J. Appl. Phys. **82**, 3874 (1997)
30. G.H. Avetisyan, V.B. Kulikov, I.D. Zalevsky, P.V. Bulaev, Proc. SPIE **2694**, 216 (1996)
31. U. Pfeiffer, M. Kneissl, B. Knüpfer, N. Müller, P. Kiesel, G.H. Döhler, J.S. Smith, Appl. Phys. Lett. **68**, 1838 (1996)
32. H.L. Vaghjiani, E.A. Johnson, M.J. Kane, R. Grey, C.C. Phillips, J. Appl. Phys. **76**, 4407 (1994)
33. P. Kiesel, K.H. Gulden, A. Hoefler, M. Kneissl, B. Knuepfer, S.U. Dankowski, P. Riel, X.X. Wu, J.S. Smith, G.H. Doehler, Proc. SPIE **1985**, 278 (1993)
34. P.K. Basu, Theory of Optical Process in Semiconductors: Bulk and Microstructures (Oxford University Press, Oxford 1997)
35. G.H. Doheler, Phys. Scr. **24**, 430 (1981)
36. S. Mukherjee, S.N. Mitra, P.K. Bose, A.R. Ghatak, A. Neoigi, J.P. Banerjee, A. Sinha, M. Pal, S. Bhattacharya, K.P. Ghatak, J. Comput. Theor. Nanosci. **4**, 550 (2007)

http://www.springer.com/978-3-642-31247-2

Effective Electron Mass in Low-Dimensional Semiconductors

Bhattacharya, S.; Ghatak, K.P.

2013, XXIV, 536 p., Hardcover
ISBN: 978-3-642-31247-2